

## Magnetic circular dichroism of the S 2*p*, Co 2*p*, and Co 3*p* core absorption and orbital angular momentum of the Co 3*d* state in low-spin CoS<sub>2</sub>

T. Muro, T. Shishidou, F. Oda, T. Fukawa, H. Yamada, A. Kimura, S. Imada, and S. Suga\*  
*Department of Material Physics, Osaka University, 1-3, Machikaneyama, Toyonaka, Osaka 560, Japan*

S. Y. Park and T. Miyahara  
*Photon Factory, National Laboratory for High-Energy Physics, Oho 1-1, Tsukuba, Ibaragi 305, Japan*

K. Sato  
*Faculty of Technology, Tokyo University of Agriculture and Technology, Koganei, Tokyo 184, Japan*  
 (Received 26 June 1995; revised manuscript received 27 November 1995)

Magnetic circular dichroism (MCD) has been measured for ferromagnetic CoS<sub>2</sub> in the S 2*p*, Co 2*p* and 3*p* core absorption regions. MCD in the S 2*p* region is discussed in terms of the exchange splitting of the unoccupied band. The Co 2*p* MCD has revealed that the orbital angular momentum of the Co 3*d* state remains finite in spite of its low-spin configuration. This situation is confirmed by a simple cluster model calculation.

### I. INTRODUCTION

Transition metal (TM) dichalcogenide compounds with pyrite structure,  $MX_2$  ( $M = \text{Mn, Fe, Co, Ni}$ ;  $X = \text{S, Se, Te}$ ), show various magnetic and electronic properties. For example, FeS<sub>2</sub> is a paramagnetic semiconductor, CoS<sub>2</sub> is a ferromagnetic metal, and NiS<sub>2</sub> is an antiferromagnetic semiconductor. Furthermore, partial substitution of the chalcogenide element strongly modifies their properties. For instance, partial substitution of S by Se rapidly decreases the Curie temperature  $T_c$  of CoS<sub>2</sub> and induces insulator-metal transition in NiS<sub>2</sub>. Thus, the chalcogen elements have significant roles in the physical properties of these materials. So, understanding of the electronic structures of TM pyrites and the contribution of chalcogen element is an interesting subject to be studied in detail.

Among them, the magnetic property of ferromagnetic CoS<sub>2</sub> was studied by a polarized neutron diffraction technique and a slight magnetic moment was reported for S.<sup>1</sup> CoS<sub>2</sub> is an itinerant ferromagnet with the Curie temperature of  $T_c \approx 120$  K. The crystal structure is pyrite-type cubic and is represented by the space group  $T_h^6(Pa3)$ . The Co atom is octahedrally surrounded by six covalently bonded S-S pairs. The Co 3*d* electrons are in the low-spin state. The saturated magnetic moment was estimated by means of neutron-diffraction measurements to be  $0.85\mu_B$  per Co atom.<sup>2</sup> Recently, the spin-dependent density of states (DOS) was calculated by using the self-consistent tight-binding method.<sup>3</sup>

It is now well known that the magnetic circular dichroism (MCD) of the core absorption spectra (XAS) done for ferromagnetic and ferrimagnetic materials with using circular polarized synchrotron-radiation light can sensitively probe the spin and/or orbital angular momentum of the electronic state involved in the absorption transition. MCD has so far been mostly measured for the core transitions to the 3*d* states in transition-metal elements and for the transitions to the 4*f* states in the rare-earth elements. In this work, we measure MCD in the anion S 2*p* excitation region of CoS<sub>2</sub> and try to

interpret the slight magnetic moment observed on the S atom. For this purpose, we compare the MCD spectrum with the band calculation and the x-ray-bremsstrahlung-isochromat-spectroscopy (X-BIS) spectrum and discuss the origin of the S 2*p* MCD signal. MCD is also measured in the Co 2*p* and 3*p* absorption regions. By analyzing the Co 2*p* MCD with use of the sum rule, we evaluate  $\langle L_z \rangle / \langle S_z \rangle$  of Co as 0.18. This result is interpreted on the basis of a simple cluster model calculation.

### II. EXPERIMENTAL

The S 2*p* and Co 3*p* MCD experiments were done at BL28A of the Photon Factory and the Co 2*p* MCD spectrum was measured at the NE1B beamline of the Accumulation Ring for Tristan in the National Laboratory for High Energy Physics, Tsukuba, Japan. Both beamlines were equipped with helical undulators and provided circularly polarized undulator radiation (more than 95% polarized). The effective photon energy ( $h\nu$ ) regions were 5–300 eV at BL28A and 500–1500 eV at NE1B.

Single crystals of CoS<sub>2</sub> were grown by the chemical vapor transport technique with chlorine gas as a transport agent.<sup>4</sup> The sample was cooled down by liquid N<sub>2</sub>. Clean surfaces were obtained by *in situ* filing. The absorption intensity was measured by means of the total photoelectron yield in the ultrahigh vacuum ( $\sim 1 \times 10^{-9}$  Torr). The measurement was performed in the Faraday geometry, i.e., with both the incident light and the magnetization perpendicular to the sample surface. We used two pairs of Nd-Fe-B permanent dipole magnets with holes for passing the excitation light.<sup>5</sup> The field of  $\sim 1.1$  T at the sample position was alternatively reversed by setting one of the two dipole magnets on the optical axis by means of a motor-driven linear feed-through. The MCD spectrum is defined as  $I_+ - I_-$ , where  $I_+(I_-)$  is the absorption for the magnetic field and the photon spin parallel (antiparallel) to each other. Here,  $I_+$  and  $I_-$  spectra were taken by reversing the magnetic field at each  $h\nu$ . For the X-BIS measurement, the clean sample sur-

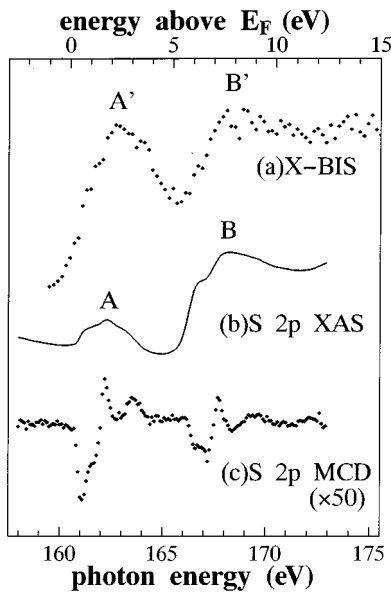


FIG. 1. (a) X-BIS spectrum of  $\text{CoS}_2$  (its energy scale is given at the top). (b) S  $2p$  XAS spectrum defined as  $(I_+ + I_-)/2$  (its energy scale is given at the bottom). (c) S  $2p$  XAS MCD spectrum,  $(I_+ - I_-) \times 50$ .

face was obtained by repeated filing under the ultrahigh vacuum ( $\sim 1 \times 10^{-10}$  Torr).

### III. RESULTS AND DISCUSSION

#### A. S $2p$ core absorption

First, we discuss the S  $2p$  XAS spectrum [Fig. 1(b)]. It is characterized by the two absorption regions, A and B, in which remarkable MCD signals [Fig. 1(c)] are observed (the magnification factor is indicated in the figure). One recognizes the similarity between the MCD structures in both regions. The MCD spectrum shows a minimum at the low energy onsets of both A and B absorption regions and maxima in higher energies. (So far, S  $1s$  XAS spectra of some pyrite-type compounds were reported<sup>6,7</sup> and the S  $1s$  XAS spectrum of  $\text{FeS}_2$  was compared with an X-BIS spectrum and the band calculation.<sup>8</sup>) The S  $2p$  core state of  $\text{CoS}_2$  is observed at 162 eV below the Fermi level ( $E_F$ ) by our photoemission spectrum. Then, the core excitation threshold to excite an electron just above  $E_F$  is expected at  $h\nu = 162$  eV. The observed absorption threshold near  $\sim 160.5$  eV and the similarity of the XAS and the X-BIS spectrum displayed in Fig. 1(a) can be well understood by considering the Coulomb interaction ( $\sim 1.5$  eV) between the S  $2p$  core hole and the excited electron in the unoccupied band. One notices, however, that the absorption intensity in the region A is relatively weaker than the X-BIS intensity in the region A'. According to the band calculations,<sup>3,8</sup> the conduction band in the region A' (B') mainly consists of the Co  $3d$  and S  $3p\sigma^*$  (S  $3d$ , Co  $4s$ , and  $4p$ ) components. Here, the  $3p\sigma^*$  molecular orbital state is formed in each S-S pair. The absorption in the region B mainly corresponds to the dipole-allowed S  $2p \rightarrow$  S  $3d$  transition. On the other hand, the weaker absorption in region A corresponds to transitions to the S  $d$ - and  $s$ -like components that have weak, but finite

partial DOS in this region. Interatomic transitions such as S  $2p \rightarrow$  Co  $3d$  and S  $2p \rightarrow$  S  $3p\sigma^*$  might have contributions to this region as well.

Then, we discuss the MCD of the S  $2p$  XAS spectra. If we consider the spin dependence of the band structures, the selection rule combined with the spin dependent DOS of the unoccupied band provides the MCD. According to the band calculation by Zhao, Callaway, and Hayashibara,<sup>3</sup> the S  $3p\sigma^*$  band has exchange splitting, due to the hybridization with the Co  $3d$  band. It is also suggested that the S  $3s$ ,  $3d$ , and  $4s$  bands have exchange splittings with the same sign as the Co  $3d$  band. Thus, the partial DOS of the S band with the spin parallel to the Co  $3d$  majority spin (hereafter called majority-spin S band) is larger than that of the minority-spin band at the onset of its unoccupied DOS. At the absorption onset, the  $2p_{3/2}$  absorption mostly contributes to the MCD, because of the S  $2p$  spin-orbit splitting ( $\sim 1$  eV). For the  $p_{3/2} \rightarrow s$  absorption, electrons with the spin parallel to the Co  $3d$  majority (minority) spin are preferentially excited in the  $I_+$  ( $I_-$ ) spectrum and, therefore, the MCD signal is expected to show a positive peak at the onset, in contrast to the experimental result. For the  $p_{3/2} \rightarrow d$  absorption, the spin preference is just opposite and the MCD spectrum should show negative sign at the onset. Hence, the MCD signals at the onsets of both A and B regions are attributed to the  $p \rightarrow d$  transition character. The relative magnitude of the MCD compared with the XAS peak height is six times smaller for the B band than for the A band. This result clarifies the appreciably smaller exchange splitting of the unoccupied band in the B region than in the A region.

#### B. Co $p$ core absorption

Next, we discuss the Co  $p$  core absorption bands. As observed in Fig. 2(a), the Co  $3p_{3/2}$  and  $3p_{1/2}$  absorption bands are mixed, because of the small spin-orbit splitting compared with the Coulomb and exchange interactions. A dip structure is observed in the energy region just below the absorption onset. This structure is caused by the Fano effect, due to an interference between the direct photoemission from the  $3d$  state and the super Coster-Kronig decay following the  $3p \rightarrow 3d$  core excitation. Therefore, the analysis of the MCD spectrum is rather difficult in this region.

In Fig. 2(b) are shown the Co  $2p_{3/2}$  and  $2p_{1/2}$  absorption and MCD spectra, in which typical positive-negative MCD spectrum is observed. Both of the  $2p_{3/2}$  and  $2p_{1/2}$  absorption peaks have satellite structures in the  $h\nu$  regions of about 6 eV higher than the main peaks. Similar satellite structures were reported for the Ni  $2p$  absorption<sup>9</sup> and well explained as charge-transfer satellites from a viewpoint of the configuration interaction on the basis of the Anderson impurity model.<sup>10</sup> However, the possibility of assigning the present satellite structures to the unoccupied bands is more plausible. For example, the X-BIS spectrum [Fig. 1(a)] shows a broadband around 8 eV above  $E_F$ . In addition, the S  $2p$  core absorption spectrum has shown an appreciable MCD in the corresponding energy region, which can be understood if the Co  $3d$  state is hybridized with the S state in this energy region. The presence of the weaker MCD signal in the Co  $2p$  absorption satellite region can be consistently explained on this band hybridization model. In the main peaks,

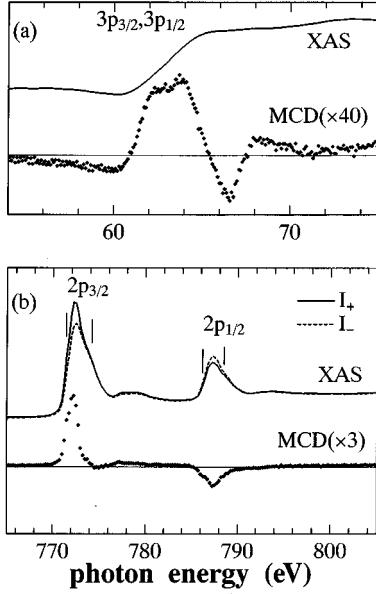


FIG. 2. (a) Co 3*p* XAS and MCD spectra. The solid line is the XAS defined as  $(I_+ + I_-)/2$  and the dots are the MCD,  $(I_+ - I_-) \times 40$ . (b) Co 2*p* XAS and MCD spectra. The solid line is  $I_+$  and the dashed line is  $I_-$ . The dots show the MCD spectrum multiplied by 3.

we can recognize some multiplet structures as indicated by the vertical bars. The MCD signals appreciably depend upon the individual multiplet and provide line shapes different from the XAS. For example, the MCD drastically decrease on the higher-energy side of the  $2p_{3/2}$  main peak. This result suggests the importance of the electron-core hole exchange and Coulomb interactions for the Co  $2p \rightarrow 3d$  excitation in addition to the itinerant character or the hybridization effect in  $\text{CoS}_2$ .

The main features of the XAS and MCD are thus interpreted by considering the  $p \rightarrow d$  transition. Next, we add some comments on the origin of the remarkable line-shape difference of the MCD spectra between the S 2*p* [Fig. 1(c)] and Co 2*p* [Fig. 2(b)] absorption. The first reason for this is the magnitude of the spin-orbit splitting of the 2*p* state. The splitting of the Co 2*p* state ( $\sim 15.5$  eV) is much larger than the absorption bandwidth, whereas that of the S 2*p* state ( $\sim 1$  eV) is smaller than that. The second and more essential reason is that the Co 3*d* substates are unevenly occupied (with leaving some orbital angular momentum) in the ground state, whereas the exchange splitting between the opposite spin unoccupied bands is playing the dominant role in the S 2*p* XAS MCD. In the case of the Co 2*p* XAS MCD, the effect of absorption intensity difference is much larger than the effect of the exchange splitting. The magnitude of the MCD signals is roughly ten times different between the S 2*p* and Co 2*p* XAS MCD. This result is a natural consequence of the two different MCD mechanisms.

It is relatively easy to analyze the MCD spectrum in the Co 2*p* core excitation region, because of the larger spin-orbit splitting and smaller interference effect in comparison with the Co 3*p* spectrum.<sup>11,12</sup> The integrated intensity ratio of the MCD signals for the  $2p_{3/2}$  and  $2p_{1/2}$  excitations is about 1.5: -1.0. By tentatively subtracting the absorption background,

TABLE I. The Slater integrals and the spin-orbit constants (in the unit of eV) obtained by reducing the Hartree-Fock values by the factors  $c$ .

	$3d^7$	$3d^8$	$3d^9$	$c$
$F^2$	9.678	8.746		0.8
$F^4$	6.010	5.394		0.8
$\zeta_d$	0.091	0.082	0.074	1.0

the  $\langle L_z \rangle$  is evaluated to be about  $0.06\mu_B$ . This evaluation, however, depends upon the background subtraction and the degree of magnetization. Therefore, we try to evaluate  $\langle L_z \rangle / \langle S_z \rangle$ , which does not explicitly depend upon such conditions as far as the magnetic dipole moment  $\langle T_z \rangle$  and the overlap between the  $2p_{3/2}$  and  $2p_{1/2}$  absorption bands are neglected. In strong contrast to the general expectation for low-spin materials that  $\langle L_z \rangle \sim 0$ ,  $\langle L_z \rangle / \langle S_z \rangle$  is estimated to be 0.18 in  $\text{CoS}_2$ .

### C. Calculation of initial state

In order to understand this result of  $\langle L_z \rangle / \langle S_z \rangle$ , we tentatively evaluate both  $\langle L_z \rangle$  and  $\langle S_z \rangle$  by calculating the ground state in a simplified cluster model consisting of one  $\text{Co}^{2+}$  ion octahedrally surrounded by six anions ( $X^{2-}$  ions are assumed instead of  $S_2^{2-}$  molecules). The Hamiltonian  $H$  is written as

$$H = H_1 + H_2, \quad (1)$$

where

$$\begin{aligned}
 H_1 = & \sum_i \varepsilon_d(\Gamma_i) \sum_{\gamma_i} d_{\gamma_i}^+ d_{\gamma_i} + \sum_i \varepsilon_p(\Gamma_i) \sum_{\gamma_i} p_{\gamma_i}^+ p_{\gamma_i} \\
 & + U_{dd} \sum_{i,j} \sum_{\gamma_i \neq \gamma_j} d_{\gamma_i}^+ d_{\gamma_i} d_{\gamma_j}^+ d_{\gamma_j} + \sum_i V(\Gamma_i) \sum_{\gamma_i} (d_{\gamma_i}^+ p_{\gamma_i} \\
 & + \text{H.c.}) + g\mu_B H \sum_i s_z(\gamma_i) d_{\gamma_i}^+ d_{\gamma_i}, \quad (2)
 \end{aligned}$$

$$H_2 = H_{d-d}(F^2, F^4) + H_d(\zeta_d). \quad (3)$$

In Eq. (2), the first and second terms describe the energies of the 3*d* and 3*p* electrons in the  $\gamma_i$  substate belonging to the  $\Gamma_i$  ( $t_{2g}$  or  $e_g$ ) irreducible representation of the  $O_h$  point group for the  $\text{CoS}_6$  cluster. The third and fourth terms represent the 3*d*-3*d* repulsive Coulomb interaction and the hybridization between the Co 3*d* and S 3*p* states. The molecular field applied on the 3*d* spin is given by the fifth term. In Eq. (3),  $H_{d-d}$  is the 3*d*-3*d* electrostatic interaction given by the Slater integrals  $F^2$  and  $F^4$ , and  $H_d$  is the spin-orbit interaction in the 3*d* state with the coupling constant  $\zeta_d$ . The  $F^0$  term is treated in the third term of Eq. (2). We used  $F^2$ ,  $F^4$ , and  $\zeta_d$  values shown in Table I obtained by reducing the Hartree-Fock values by the factors  $c$ . The initial state is assumed to be a linear combination of the  $3d^7$ ,  $3d^8\bar{L}$ , and  $3d^9\bar{L}^2$ . We have used the following parameter values (in the unit of eV):  $10Dq = 3$ ,  $g\mu_B H = 0.2$ ,  $\Delta = 2.5$ ,<sup>13</sup>  $U_{dd} = 4.2$ ,<sup>13</sup>  $V_{t_{2g}} = -1.3$ ,<sup>14</sup>  $V_{e_g} = 2.4$  (Ref. 14) (here,  $V_{t_{2g}}$  and  $V_{e_g}$  are

$m_l$	$m_s \uparrow$		$m_s \downarrow$	
	2	50	50	54
1	100	100	100	100
0			13	61
-1	100	100	100	100
-2	50	50	59	80

(a) (b)

FIG. 3. The occupation probability of the Co 3d one-electron orbitals in the low-spin state depending on the magnetic quantum numbers of spin angular momentum ( $m_s$ ) and orbital angular momentum ( $m_l$ ). (a) is for the  $d^6$  state and (b) is the calculated result for the 3d state ( $d^{7.47}$ ) in the CoS<sub>6</sub> cluster model.

taken from the values for pyrite-type NiS<sub>2</sub>). Here,  $10Dq [= \varepsilon_d(e_g) - \varepsilon_d(t_{2g})]$  is the crystal-field splitting and  $\Delta$  is the charge-transfer energy as the average energy difference  $E(3d^8\bar{L}) - E(3d^7)$ . We have then obtained  $\langle S_z \rangle = 0.49\mu_B$  and  $\langle L_z \rangle = 0.05\mu_B$ , which provides a value of  $\langle L_z \rangle / \langle S_z \rangle = 0.10$ . Although this value is slightly smaller than the experimental evaluation (0.18), the essential result of finite  $\langle L_z \rangle$  is established. The  $\langle L_z \rangle + 2\langle S_z \rangle$  is  $1.03\mu_B$  in this calculation, which is slightly larger than the experimental value of  $0.85\mu_B$ . The deviations of  $\langle L_z \rangle + 2\langle S_z \rangle$  and  $\langle L_z \rangle / \langle S_z \rangle$  from the experimental values are not astonishing, because the employed parameters are rather tentative.

The occupation probability of the Co 3d ( $m_l, m_s$ ) states is given in Fig. 3(b) and compared with that in the (a)  $d^6$  configuration. The residual orbital angular momentum is due to the unbalance in the occupation of the  $m_l = 2$  ( $Y_{22}$ ) and  $m_l = -2$  ( $Y_{2-2}$ ) states, which is induced by the interplay

of the spin-orbit interaction and the mixing between the  $d_{xy}$  and  $d_{x^2-y^2}$  orbitals [represented as  $-i(Y_{22} - Y_{2-2})/\sqrt{2}$  and  $(Y_{22} + Y_{2-2})/\sqrt{2}$ ]. This mixing is caused by the off-diagonal matrix element of the electrostatic Coulomb and exchange interactions.

#### IV. CONCLUSIONS

In conclusion, remarkable MCD spectrum is found in the anion S 2p absorption region of ferromagnetic CoS<sub>2</sub>. The similarity of the features between the S 2p XAS and X-BIS spectra and the resemblance of the MCD structures in the A and B regions strongly suggest the contribution of the spin-polarized DOS of the unoccupied band, due to the hybridization with the Co 3d state. The satellite structures of both the Co 2p XAS and MCD spectra are also understood on this model. The Co 2p MCD spectrum has revealed the finite  $\langle L_z \rangle / \langle S_z \rangle$ . The finite  $\langle L_z \rangle$  is reproduced by the simplified cluster calculation and attributed to the mixing between the  $d_{xy}$  and  $d_{x^2-y^2}$  orbitals. So far, the MCD measurements have mostly been applied to the excitation of magnetic atoms in ferromagnetic compounds. But studies of the interaction between the magnetic atom and the nonmagnetic atom are very important for understanding the magnetic character of ferromagnetic compounds. This experiment demonstrates a possibility of comprehensive interpretation of the magnetic character of ferromagnetic compounds by means of the MCD measurement.

#### ACKNOWLEDGMENTS

The authors would like to thank Professor A. Fujimori and Professor T. Kanomata for fruitful discussions. They are also much obliged to Dr. G. L. Zhao for useful suggestion about his band calculation. One of the authors (T.S.) would like to thank Mr. A. Tanaka and Professor T. Jo for information on the Lanczos method and numerical programming.

\*Author to whom correspondence should be addressed.

<sup>1</sup>A. Ohsawa, Y. Yamaguchi, H. Watanabe, and H. Itoh, J. Phys. Soc. Jpn. **40**, 992 (1976).

<sup>2</sup>K. Adachi, K. Sato, and M. Takeda, J. Phys. Soc. Jpn. **26**, 631 (1969).

<sup>3</sup>G. L. Zhao, J. Callaway, and M. Hayashibara, Phys. Rev. B **48**, 15 781 (1993).

<sup>4</sup>K. Sato and T. Teranishi, J. Phys. Soc. Jpn. **50**, 2069 (1981).

<sup>5</sup>S. Muto, Y. Kagoshima, and T. Miyahara, Rev. Sci. Instrum. **63**, 1470 (1992).

<sup>6</sup>C. Sugiura, J. Chem. Phys. **74**, 215 (1981).

<sup>7</sup>T. Matsukawa, M. Obashi, S. Nakai, and C. Sugiura, Jpn. J. Appl. Phys. Suppl. **17-2**, 184 (1978).

<sup>8</sup>W. Folkerts, G. A. Sawatzky, C. Haas, R. A. de Groot, and F. U. Hillebrecht, J. Phys. C **20**, 4135 (1987).

<sup>9</sup>C. T. Chen, F. Sette, Y. Ma, and S. Modesti, Phys. Rev. B **42**, 7262 (1990).

<sup>10</sup>T. Jo and G. A. Sawatzky, Phys. Rev. B **43**, 8771 (1991), and references therein.

<sup>11</sup>B. T. Thole, P. Carra, F. Sette, and G. van der Laan, Phys. Rev. Lett. **68**, 1943 (1992).

<sup>12</sup>P. Carra, B. T. Thole, M. Altarelli, and X. Wang, Phys. Rev. Lett. **70**, 694 (1993).

<sup>13</sup>A. E. Bocquet, T. Mizokawa, T. Saitoh, H. Namatame, and A. Fujimori, Phys. Rev. B **46**, 3771 (1992).

<sup>14</sup>K. Mamiya, Master thesis, University of Tokyo, 1994.